

DOI: 10.1002/sml.200500314

Directed Fabrication of Radially Stacked Multifunctional Oxide Heterostructures Using Soft Electron-Beam Lithography

Zixiao Pan, Suresh K. Donthu, Nianqiang Wu, Shuyou Li, and Vinayak P. Dravid*

A versatile patterning approach based on electron-beam lithography (eBL) and solution deposition, termed soft-eBL, has been developed to fabricate radially stacked heterostructures of multifunctional oxides from their sol precursors. Well-defined nanorings of lead zirconate titanate (PZT) are fabricated on a variety of substrates such as noble metals (e.g., Au), semiconductors (e.g., Si), and oxide single crystals (e.g., SrTiO₃), which were previously functionalized with appropriate self-assembled monolayers (SAMs). The undercut in the double-layer eBL resist and substrate functionalization with the SAM treatment play a vital role in the formation of the ring structures. The nanorings are then used as building block “containers” and ring-reservoirs are filled with a second sol (e.g., CoFe₂O₄) to form radially stacked composite ceramic heterostructures. The approach presented here does not require either feature alignment to realize heterostructures or the etching of ceramics, and is amenable to a variety of radially stacked composite heterostructures.

Keywords:

- electron-beam lithography
- heterostructures
- nanostructures
- oxides
- self-assembled monolayers

1. Introduction

The past decade has witnessed the emergence of diverse techniques for patterning a wide variety of molecular and “soft” nanostructures within a two-dimensional (2D) regime.^[1–4] However, as the nanostructure paradigm shifts from monolithic single-phase materials and planar geometry to complex compounds and stacked 3D architectures, there is a continuing need for advancing the nonplanar stacking of solid-state structures, especially for multifunctional materials, in a patterned geometry. Heterostructures composed

of multifunctional oxides (e.g., multilayer structures) exhibit a fascinating breadth of properties for applications such as microelectromechanics,^[5] optoelectronics,^[6,7] microwave devices,^[8] and data storage,^[9] among many others, based on the interaction between different phases when stimulated by external fields. Recently, vertically aligned heterostructures (such as nanopillars of one phase embedded in the matrix of another)^[10,11] have attracted considerable attention as these nanostructures significantly enhance such interactions. While these vertical heterostructures are fabricated using a phase-separation-based self-assembly approach, a patterning technique that affords controlled dimensions and the separation of such minute structures is highly desirable.

There are considerable challenges in fabricating nonplanar ceramic heterostructure nanopatterns using current “top-down” patterning techniques, which are better suited for the fabrication of single-component 2D structures. The key bottleneck is the stringent requirement on feature re-

[*] Z. Pan, S. K. Donthu, Dr. N. Wu, Dr. S. Li, Prof. V. P. Dravid
Department of Materials Science and Engineering
International Institute of Nanotechnology
Northwestern University, Evanston, IL, 60208 (USA)
Fax: (+1) 847-467-6573
E-mail: v-dravid@northwestern.edu

Supporting information for this article is available on the WWW under <http://www.small-journal.com> or from the author.

alignment between the multiple patterning steps,^[4,12–14] which are required in order to form nonplanar patterns composed of more than two materials. Such a constraint is particularly critical for nanometer-sized structures as it allows alignment precision at a relatively small scale. Methods such as polymer phase separation,^[15] templated growth,^[16] interference lithography,^[17] and nanotransfer printing^[4] have been developed for fabricating nonplanar nanostructures without the need for high-precision feature alignment. However they are demonstrated mainly for metals and polymers, and are not well suited for ceramics. Direct deposition methods such as robotic deposition^[18] enable the fabrication of intricate ceramic structures, yet there are restrictions on the deposition environment and the smallest feature size attainable.

The refractory nature and chemical inertness of ceramics also pose challenges to patterning. The sophisticated electron-beam lithography (eBL) technique can readily generate sub-10 nm features on polymeric resist, yet when used to prepare ceramic patterns by sputtering, it is difficult to avoid etching processes in order to lift off the patterns. This may lead to severe problems such as sidewall redeposition, contamination, and structural damage.^[19] The electron-beam direct-writing approach^[20,21] is an alternative that circumvents the etching problems by using e-beam-sensitive sol precursors as resist. This technique maintains the high resolution of traditional electron-beam lithography and was shown to generate very fine ceramic features.^[22] However the sensitivity of these sol precursors is usually much lower than dedicated polymer resists, and a relatively higher dose is required for material exposure.^[22,23] On the other hand, although “bottom-up” methods that utilize self-organization or the self-assembly of materials do not involve etching, stacking of two or more different oxides into heterostructured patterns has not been well explored. Difficulties for bottom-up methods also exist in precisely controlling the shape, size, and relative position of the nanocomponents.^[24] Therefore, patterning nonplanar ceramic heterostructures still faces considerable challenges for either an entirely top-down or an entirely bottom-up patterning process.

Here we present a versatile approach for patterning radially stacked multifunctional oxide heterostructures without the need for feature alignment or etching. The approach is based on the “soft-eBL” technique recently developed in our group, which is particularly well-suited for fabricating ceramic nanostructures.^[25] Here, ring structures of one inorganic material with ring widths less than 100 nm are first fabricated from its sol precursor by modifying the solvophobicity of substrates by using appropriate self-assembled monolayers (SAMs). Such rings are then utilized as building-block “containers” by filling them with a second sol to form radially stacked “core-shell” heterostructure patterns. This directed patterning of oxide heterostructures is successfully achieved on diverse substrates with control over their dimensions, and it avoids a painstaking feature-alignment procedure between patterning of the first and second materials. This contribution demonstrates the efficacy and feasibility of fabricating radially stacked core-shell heterostructures via soft-eBL.

2. Results and Discussion

The soft-eBL technique is a combination of electron-beam lithography and the spin-coating of liquid precursors, as schematically shown in Figure 1 A (see Experimental Sec-

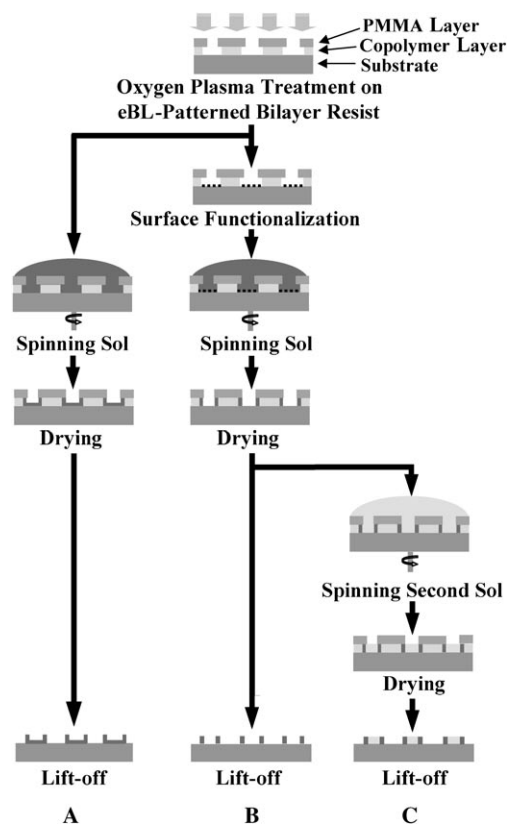


Figure 1. The soft-eBL process: A) For developing barrel structures. B) For developing nanoring structures. C) For developing radially stacked heterostructures.

tion for details). In a typical run, the substrate was spin-coated with a bilayer electron-beam resist consisting of a methyl methacrylate (MMA) and methacrylic acid (MAA) copolymer at the bottom, and a polymethyl methacrylate (PMMA) layer on the top, each with a nominal thickness of about 150 nm. The higher electron-beam sensitivity of the copolymer as compared to PMMA enables excellent lift-off in a bilayer configuration, and plays a critical role in controlling the geometry of the fabricated nanostructures, as elaborated below. The resist-coated substrates were electron-beam patterned with an array of circular (1 μm diameter) or square discs (1 \times 1 μm). After being developed, the patterned substrates were treated with an oxygen plasma to remove any organic residue left in the patterned area and to increase the hydrophilicity of the resist to enable filling of the patterned discs with aqueous sol. Subsequently, a PZT sol (0.1 M) was spun on to the patterned substrates at between 4000 and 6000 rpm for 40 s and the samples were immediately heated at 150 $^{\circ}\text{C}$ for 5 min to gelate the patterns. The samples were then soaked in acetone to dissolve the

resist and to lift-off excess sol material from the unpatterned areas.

The square patterns of PZT fabricated on platinized silicon substrates using the soft-eBL approach after spinning the substrates at 6000 rpm are shown in Figure 2. The

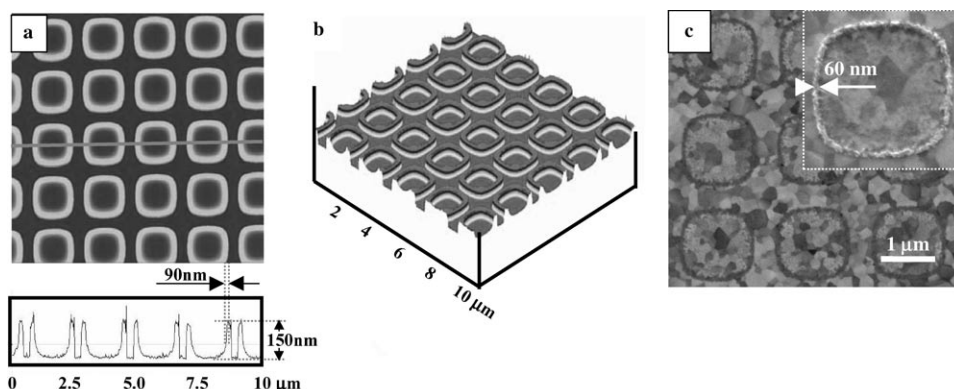


Figure 2. PZT rings on platinized silicon substrate: a) AFM topographic image and cross-sectional analysis of PZT rings before annealing; b) AFM 3D construction of the rings; c) SEM backscattered electron image of PZT rings annealed at 600 °C for 1 h (the inset shows a secondary electron image of a ring).

atomic force microscopy (AFM) topographic images and the cross-sectional profile in Figure 2 a and b indicate that the square patterns have in fact developed into barrel shapes; these images are analogous to snap-shots of liquid in a spinning beaker. Each barrel has a wall thickness of about 90 nm and a height of 150 nm, as analyzed from the AFM profiles. After annealing this sample at 600 °C for 1 h in air, the wall thickness was reduced by nearly 30% to about 60 nm. Scanning electron microscopy (SEM) images of the annealed patterns are shown in Figure 2c. Note that the grain size of the bottom Pt substrate, inside as well as outside of the pattern, can be observed from the backscattered electron (BSE) image. However, the secondary electron (SE) image in the inset shows residual islands of PZT at the bottom of the barrels and that the substrate surface is not completely clean. We suggest that a certain amount of the sol material is expelled out of the air holes when spin-coated at 6000 rpm due to high centrifugal forces, and the remaining sol preferentially accumulates at the walls of the discs, driven by the capillary force. The thin layer of sol left on the inside surface is likely due to the hydrophilic nature of the Pt surface. A similar phenomenon was observed when dipping a porous membrane in alcohol-based sols, where cuplike structures are formed on hydrophilic supporting substrates and ring structures on relatively hydrophobic substrates.^[26] This result hints that by varying the surface property of the exposed substrate area, the shape of the ceramic structures can be tuned. Further, building radially stacked heterostructure patterns would be possible if the bottom center of the patterns are made free of spin-coated material to attain a pure (bottomless) ring geometry. By simply filling the rings with another functional oxide sol, columnar core-shell architectures can be fabricated without the need for painstaking realignment and multistep patterning.

2.1. Surface Modification and Fabrication of Ring Reservoirs

One way to keep the substrate surface inside of the ring free of sol material is to increase the contact angle of the sol with the substrate, which can be achieved through chemical

modification using SAMs.^[27–30] For example, 1-octadecanethiol (ODT) and octadecanetrichlorosilane (OTS) can effectively increase the contact angle of water or alcohol on noble metal and silicon oxide surface, respectively.^[29,30] Further, the SAM-modification procedure is compatible with the soft-eBL approach. Therefore, SAMs were utilized after developing the patterns in e-beam resist and using oxygen plasma treatment to render a hydrophobic substrate surface and thus

pure ring structures, as shown in Figure 1B. Si substrates (with a 60-nm layer of thermal oxide) were functionalized with OTS, while Au-coated substrates (30-nm-thick Au sputter-coated Si substrates with a 5 nm Ti adhesion layer) were functionalized with ODT. The treated substrates were immediately used for spin-coating a PZT sol. The subsequent steps are the same as in Figure 1A. Sol patterning was performed on the same substrate but without SAM treatment for control experiments.

The AFM topographic images and cross-sectional profiles of PZT structures on unmodified and ODT-modified Au/Ti/SiO₂/Si substrates are shown in Figure 3a and b, respectively. From cross-sectional profiles it can be noted that PZT structures form as barrels on unmodified substrates with a thick film of nearly 50 nm at the center of each barrel. In contrast, the ODT-modified surface generates a pure ring structure with the same height inside as well as outside of each ring. Chemical maps were obtained using secondary ion mass spectroscopy (SIMS) to further confirm the absence of PZT at the bottom of the rings. The Ti⁺ ion map of the pattern in Figure 3c clearly shows that the interior of each ring is devoid of any PZT material, and therefore validates the AFM results. Similar results have been observed on OTS-modified Si wafers, as shown in Figure 4a and b, where both AFM and SIMS images offer clear evidence for the PZT ring formation. Besides the modification on noble metal and Si substrates, we have also extended this approach to complex oxide substrates such as SrTiO₃ (STO) single crystals. Such perovskite-structured substrates have excellent structural compatibility with PZT and may provide control over PZT crystallography (e.g., high texture or epitaxy).^[31–34]

It should be noted that SAM formation on complex oxides has been scarcely reported, probably due to the bonding difficulty between the head groups of the organic

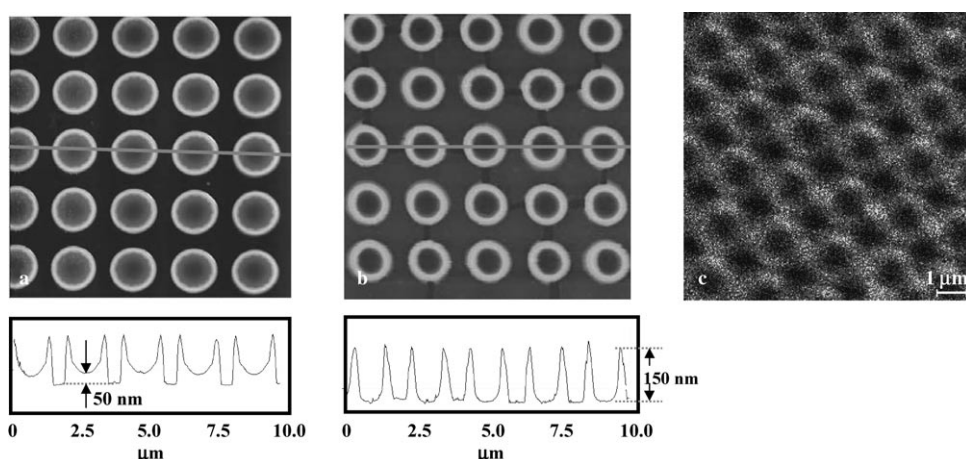


Figure 3. The effect of Au-surface functionalization on PZT ring formation using an ODT SAM. a) AFM image of PZT patterns on bare Au. The patterns developed into a barrel shape after drying, leaving 50-nm-thick PZT at the center of the bottom of the ring; b) AFM image of PZT rings formed on an ODT-modified Au surface; c) a SIMS Ti^+ map further confirms the pure ring-structure formation. The rings appear to be connected due to the shadowing effect from the restriction of the incident angle and the probe size of the ion beam.

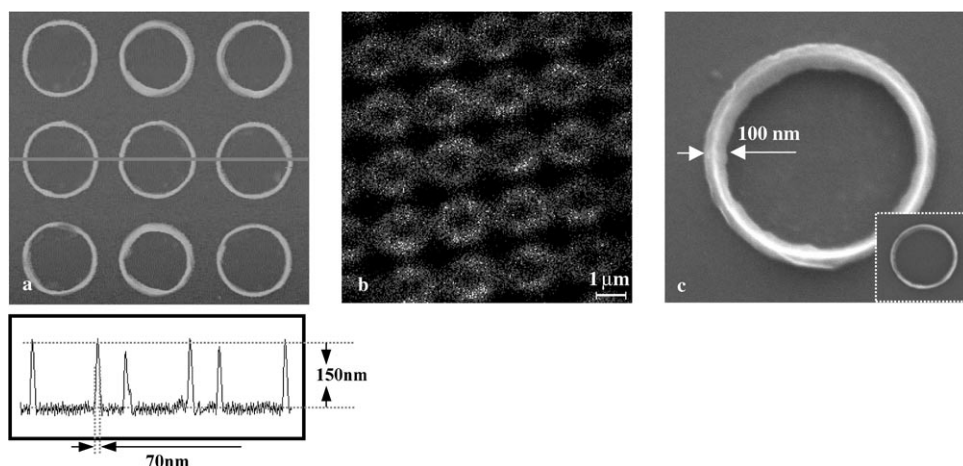


Figure 4. a) AFM topographic image and cross-sectional profile of PZT rings formed on an OTS-modified Si wafer; b) a SIMS Ti^+ map further confirms the pure ring-structure formation; c) SEM secondary electron image of PZT ring structure on an OTS-modified single-crystal SrTiO_3 substrate (the inset shows the back-scattered electron image).

molecule and the complex oxide surfaces. Nonetheless, we have attempted to increase the hydrophobicity of STO single crystals using the same SAM treatment as for Si substrates, considering that a layer of $-\text{OH}$ groups readily form on STO surfaces and may facilitate SAM formation through a reaction with trichlorosilane.^[35] Furthermore, the oxygen plasma treatment utilized in this method may help increase the density of hydroxyl groups on oxide surfaces,^[35,36] and even facilitate the $-\text{OH}$ group to be preferentially oriented,^[37] both of which can promote the silane-hydroxyl reaction. Although the bonding density may be lower than that for the silane/Si case, they may still be effective in changing the surface energy, even if a partial monolayer is formed. Therefore we patterned PZT structures on STO single-crystal substrates by using the process shown in Figure 1 B. Fig-

ure 4c shows SEM images of a PZT ring on OTS-treated STO crystal substrate demonstrating the effectiveness of OTS treatment on the ring-structure formation. We have also succeeded in patterning PZT rings on a SiN_x surface using this approach. These collective results demonstrate the effectiveness and broad applicability of substrate functionalization with SAMs as an approach to realize pure oxide rings with nanoscale width on a variety of substrates, starting from micrometer-sized prior patterns. Our experiments have shown that the process is highly reproducible and can be readily used to pattern areas as large as 1 mm^2 .

Besides the surface modification through SAM treatment, the eBL undercut also plays an important role in defining the geometry of the ring structure. The undercut profile is created due to the higher e-beam sensitivity of the bottom copolymer layer compared to the top PMMA layer. Figure 5 shows the cross-sectional SEM image of the bilayer resist after eBL patterning and development. The undercut length, defined as

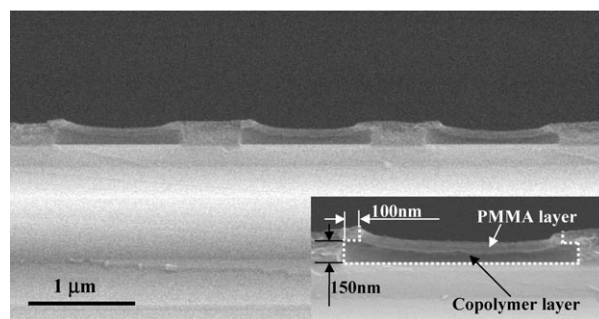


Figure 5. eBL undercut profile in the bilayer resist. The white dotted line in the inset schematically shows the edge of the profile. The thickness of the copolymer layer is 150 nm and the undercut length is 100 nm.

the length of the PMMA layer overhanging the copolymer layer, is about 100 nm, which is close to the width of the PZT rings shown in Figures 2–4. In addition, the thickness of the PMMA and the copolymer is about 150 nm each, which is remarkably close to the height of the PZT rings. This suggests the following explanation for the formation of ring structures.

The undercut profile functions in a way analogous to an aperture on top of a barrel. It allows part of the sol to be expelled under high rotational speeds, yet retains the remaining sol, which is pushed to the perimeter of each disc and preferentially accumulates there due to the solvophobicity of the bottom surface to form the ring structures after drying. Thus, the PZT ring height is determined by the thickness of the copolymer layer and the width is defined by the undercut length. We have further confirmed the above model through control experiments. When a 300-nm-thick PMMA single layer was used instead of a bilayer of the same thickness and patterned using the process shown in Figure 1B, wherein substrates are treated with SAMs, nearly 90% of the patterned area was devoid of ring structures. Moreover, the height and thickness distributions of the rings in the rest area were nonuniform (image not shown). The low yield and poor geometric uniformity therefore underscore the significance of the undercut.

particularly for a “vertically aligned” geometry.^[11,43] The patterning procedure for the heterostructure formation is illustrated in Figure 1C. PZT was first spun at 6000 rpm on SAM-treated substrates and heated at 150 °C for 5 min to generate PZT rings. This was immediately followed by cooling the substrate and spinning the CoFe₂O₄ sol at 5000 rpm to fill the PZT rings. The lower spinning speed for the core material was used because it yields a smaller centrifugal force on the spinning liquid, and thus results in a larger bottom thickness of the barrels after drying. The substrates were then heated to 150 °C again and soaked in acetone to

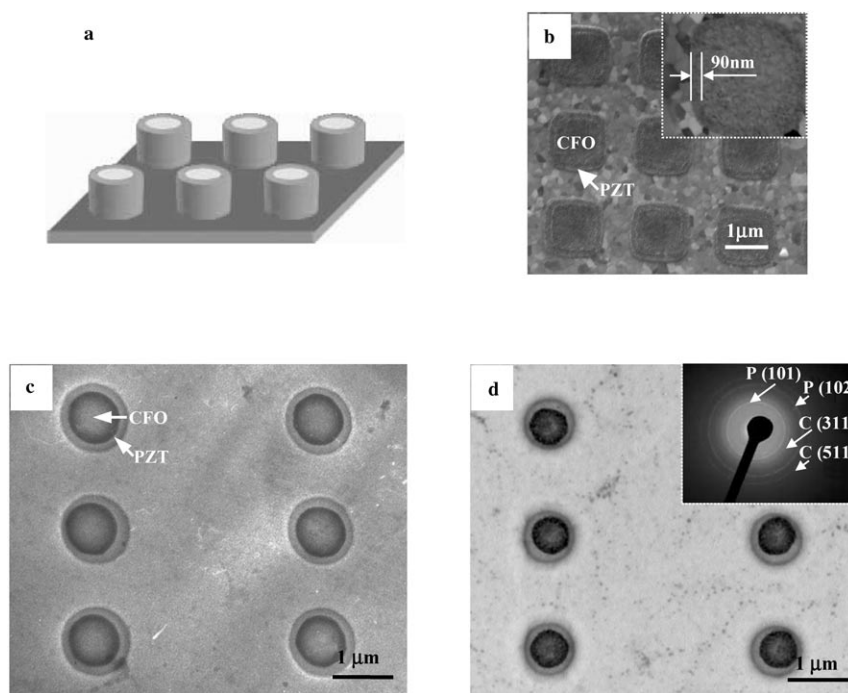


Figure 6. Radially stacked PZT/CFO heterostructure patterns fabricated using the PZT rings as building block “containers”: a) Schematic illustration of the columnar core–shell structure; b) SEM image of PZT shells/CFO cores on Pt after annealing (the inset is the BSE image showing contrast between the core and shell materials, with white lines indicating the edge of the PZT shell); c, d) TEM images of PZT shell/CFO core heterostructures on an amorphous Si_xN_y membrane, before (c) and after annealing (d) at 750 °C for 1.5 h in air (the inset shows the electron diffraction pattern taken from one core–shell pattern, where “P” stands for PZT (tetragonal phase) and “C” for CFO).

2.2. Fabrication of Radially Stacked Heterostructures

Based on the controlled formation of the nanoscale rings, radially stacked vertical heterostructure patterns were developed by simply spinning the sol of a second material to fill the rings and form the “core”, and this process can be repeated for additional radial stacking. We chose CoFe₂O₄ (CFO) as the core material due to its high magnetostrictivity and relatively high Néel temperature.^[38] Also, CFO and PZT have commensurate lattice parameters ($a_{\text{CFO}} \approx 2a_{\text{PZT}}$).^[39] This innate structural compatibility between the two phases with large magnetostriction or electrostriction (i.e., piezoelectricity) can enhance magnetoelectric coupling effects when made into appropriately aligned heterostructures,^[40–42]

lift off material outside patterned areas. Figure 6a and b show a schematic illustration and a SEM image of such columnar core–shell heterostructures (on a Pt/SiO_x/Si substrate, annealed at 700 °C for 1 h). The inset BSE image shows the average atomic number contrast between the core and the shell materials. The PZT shell is around 90 nm thick. Similar heterostructures have been fabricated on SiN_x surfaces treated with OTS. The TEM images taken before (Figure 6c) and after annealing (Figure 6d) at 750 °C in air for 1.5 h further corroborate the core–shell geometry. The average width of the shell is about 90 nm after annealing. An electron diffraction pattern taken from one of the heterostructure patterns (Figure 6d, inset) shows polycrystalline rings, and the diffraction rings correspond well to PZT (tet-

agonal phase) and CFO. This indicates that both the core and the shell materials have crystallized after annealing, and thus demonstrate the feasibility of this approach in preparing solid heterostructures with appropriate ceramic phases. There is no hint of a third phase in the diffraction profile, suggesting the phase purity of the heterostructures. Since the interface between the piezoelectric and the magnetic materials play vital roles in their interaction (which allows such heterostructure patterns to function), more detailed studies on the microstructure of each phase and the interdiffusion between the core and the shell materials are required and are in progress.

These collective results reveal a facile and general route to fabricating oxide heterostructure patterns with excellent control over pattern dimensions from both bottom-up and top-down directions: SAM treatment determines the pattern shape (i.e., ring or barrel), while the high-resolution eBL and the undercut profile simultaneously provide more rigorous control over the dimensions of the structure (i.e., thickness and height of the shell, diameter of the core, and so on). It does not require painstaking feature realignment between steps to generate the shell and to place the core inside the sub-100-nm-thick shell, and the simple spin-coating technique used eliminates the need for subsequent etching. This basic approach can be further extended to fabricate other radially stacked structures (e.g., concentric multi-ring patterns) if the appropriate spinning speed and optimal substrate-surface property control can be utilized. On the other hand, in addition to patterning on different substrates, we also patterned heterostructures of different oxide systems such as ZnO/PZT and BaTiO₃/CFO. This approach should be broadly applicable to patterning solid-state structures from any appropriate solution (e.g., sols, liquid-phase polymer precursors, and colloid particle suspensions^[44,45]) that is compatible with e-beam resists.

3. Conclusions

In summary, we have developed a broadly applicable and facile approach for patterning single-component ceramic nanostructures as well as radially stacked ceramic heterostructures from liquid-phase materials using the soft-eBL technique. By carefully controlling the surface solvophobicity with SAM treatment, this method enables the generation of nanoscale elements from micrometer-sized patterns. PZT rings with widths smaller than 100 nm were first prepared on various substrates including Au, SiO_x, SiN_x, and single-crystal STO. The undercut geometry and SAM treatment are critical for ring formation. Columnar core-shell-type heterostructures were then fabricated by filling such rings with a CFO sol. This two-step soft-eBL-based approach enables the patterning of radially stacked heterostructures of important multifunctional oxides without the need for feature realignment or etching steps, which may prove valuable for the design of new functional materials and devices.

4. Experimental Section

Substrates were spin-coated first with a MMA-MAA copolymer (MMA (8.5) MAA EL6, MicroChem Corp., USA) and then PMMA (950 PMMA A3, MicroChem Corp., USA). The bilayer resist was patterned using a Quanta 600F eBL system (FEI Company, USA) at 30 kV. The same instrument was used for imaging the patterns. Oxygen plasma treatment on the patterned substrates was performed under 75 W rf power, a 50 sccm O₂ flow rate, and a 75 torr backpressure for 20 s.

A Pb(Zr_{0.3}Ti_{0.7})O₃ (PZT) sol was prepared as described elsewhere.^[25] The 0.1 M CFO sol was prepared by dissolving appropriate portions of Co(CH₃COO)₂·4H₂O and Fe(NO₃)₃·9H₂O in 2-methoxyethanol, with 10 vol.% ethanolamine as a complexing agent. The solution was refluxed at 70 °C for 4 h, cooled, filtered, and applied to soft-eBL. Both as-prepared sols were clear and were stable for more than six months.

SAM modification of the patterned substrates was carried out by immersing the Au-coated substrates in a 3 mM ODT-isopropanol solution for 3 h and the bare Si substrates in 5 mM an OTS-anhydrous hexane solution for 20 h. The substrates were then thoroughly rinsed with the corresponding solvents, blown dry with nitrogen, and immediately used to form ring patterns.

The patterned structures were characterized using SEM (Quanta 600F, FEI Company, USA), TEM (H-8100, Hitachi, Japan), AFM (Nanoscope III microscope, Digital Instruments, USA), and SIMS (PHI TRIFT III, Physical Electronics, USA).

Acknowledgements

We acknowledge the Nanoscale Science and Engineering Initiative of the National Science Foundation (under NSF-MRC Award Number EEC-0118025), and the U.S. Department of Energy (DOE-BES) for support of this research. This work was performed in the NIFTI and EPIC facilities of the NUANCE Center at Northwestern University. The NUANCE Center is supported by NSF-NSEC, NSF-MRSEC, Keck Foundation, the State of Illinois, and Northwestern University.

- [1] P. Pammer, R. Schlapak, M. Sonnleitner, A. Ebner, R. Zhu, P. Hinterdorfer, O. Hoglinger, H. Schindler, S. Howorka, *ChemPhys-Chem* **2005**, *6*, 900–903.
- [2] J. Wang, X. Y. Sun, L. Chen, L. Zhuang, S. Y. Chou, *Appl. Phys. Lett.* **2000**, *77*, 166–168.
- [3] M. Su, M. Aslam, L. Fu, N. Q. Wu, V. P. Dravid, *Appl. Phys. Lett.* **2004**, *84*, 4200–4202.
- [4] S. Jeon, E. Menard, J. U. Park, J. Maria, M. Meitl, J. Zaumseil, J. A. Rogers, *Adv. Mater.* **2004**, *16*, 1369–1373.
- [5] R. Poyato, M. L. Calzada, L. Pardo, *J. Appl. Phys.* **2005**, *97*, 034108.
- [6] A. Nakamura, J. Ishihara, S. Shigemori, K. Yamamoto, T. Aoiki, H. Gotoh, J. Temmyo, *J. Appl. Phys.* **2005**, *44*, L4–L6.
- [7] S. V. Kalinin, D. A. Bonnell, T. Alvarez, X. J. Lei, Z. H. Hu, R. Shao, J. H. Ferris, *Adv. Mater.* **2004**, *16*, 795–799.

- [8] S. B. Majumder, M. Jain, A. Martinez, R. S. Katiyar, F. W. Van Keuls, F. A. Miranda, *J. Appl. Phys.* **2001**, *90*, 896–903.
- [9] C. H. Ahn, K. M. Rabe, J. M. Triscone, *Science* **2004**, *303*, 488–491.
- [10] V. Moshnyaga, B. Damaschke, O. Shapoval, A. Belenchuk, J. Faupel, O. I. Lebedev, J. Verbeeck, G. Van Tendeloo, M. Mucksch, V. Tsurkan, R. Tidecks, K. Samwer, *Nat. Mater.* **2003**, *2*, 247–252.
- [11] H. Zheng, J. Wang, S. E. Lofland, Z. Ma, L. Mohaddes-Ardabili, T. Zhao, L. Salamanca-Riba, S. R. Shinde, S. B. Ogale, F. Bai, D. Viehland, Y. Jia, D. G. Schlom, M. Wuttig, A. Roytburd, R. Ramesh, *Science* **2004**, *303*, 661–663.
- [12] K. Aoki, H. T. Miyazaki, H. Hirayama, K. Inoshita, T. Baba, N. Shinya, Y. Aoyagi, *Appl. Phys. Lett.* **2002**, *81*, 3122–3124.
- [13] S. Noda, K. Tomoda, N. Yamamoto, A. Chutinan, *Science* **2000**, *289*, 604–606.
- [14] B. Morgan, C. M. Waits, R. Ghodssi, *Microelectron. Eng.* **2005**, *77*, 85–94.
- [15] M. Park, C. Harrison, P. M. Chaikin, R. A. Register, D. H. Adamson, *Science* **1997**, *276*, 1401–1404.
- [16] H. O. Jacobs, A. R. Tao, A. Schwartz, D. H. Gracias, G. M. Whitesides, *Science* **2002**, *296*, 323–325.
- [17] I. Divliansky, T. S. Mayer, K. S. Holliday, V. H. Crespi, *Appl. Phys. Lett.* **2003**, *82*, 1667–1669.
- [18] J. E. Smay, J. Cesarano, J. A. Lewis, *Langmuir* **2002**, *18*, 5429–5437.
- [19] S. Clemens, T. Schnell, A. Hart, F. Peter, R. Waser, *Adv. Mater.* **2005**, *17*, 1357–1361.
- [20] S. Okamura, Y. Yagi, A. Kakimi, S. Ando, K. Mori, T. Tsukamoto, *Jpn. J. Appl. Phys. Part 1* **1996**, *35*, 5224–5228.
- [21] M. Alexe, C. Harnagea, W. Erfurth, D. Hesse, U. Gosele, *Appl. Phys. Lett.* **2000**, *70*, 247–251.
- [22] M. S. M. Saifullah, K. R. V. Subramanian, E. Tapley, D. J. Kang, M. E. Welland, M. Butler, *Nano Lett.* **2003**, *3*, 1587–1591.
- [23] J. T. Rantala, R. S. Penner, S. Honkanen, J. Vahakangas, M. Fallahi, N. Peyghambarian, *Thin Solid Films* **1999**, *345*, 185–187.
- [24] P. M. Mendes, J. A. Preece, *Curr. Opin. Colloid Interface Sci.* **2004**, *9*, 236–248.
- [25] S. K. Donthu, Z. Pan, B. Myers, G. S. Shekhawat, N. Wu, V. P. Dravid, *Nano Lett.* **2005**, *5*, 1710–1715.
- [26] H. Xu, W. A. Goedel, *Angew. Chem.* **2003**, *115*, 4845–4848; *Angew. Chem. Int. Ed.* **2003**, *42*, 4696–4700.
- [27] J. C. Love, L. A. Estroff, J. K. Kriebel, R. G. Nuzzo, G. M. Whitesides, *Chem. Rev.* **2005**, *105*, 1103–1169.
- [28] A. Sethuraman, M. Han, R. S. Kane, G. Belfort, *Langmuir* **2004**, *20*, 7779–7788.
- [29] R. K. Smith, P. A. Lewis, P. S. Weiss, *Prog. Surf. Sci.* **2004**, *75*, 1–68.
- [30] A. Pallandre, K. Glinel, A. M. Jonas, B. Nyssen, *Nano Lett.* **2004**, *4*, 365–371.
- [31] A. D. Li, Q. Y. Shao, Y. J. Wang, C. L. Mak, K. H. Wong, D. Wu, N. B. Ming, *Mater. Res. Bull.* **2001**, *36*, 2667–2675.
- [32] A. A. Talin, S. M. Smith, S. Voight, J. Finder, K. Eisenbeiser, D. Penunuri, Z. Yu, P. Fejes, T. Eschrich, J. Curless, D. Convey, A. Hooper, *Appl. Phys. Lett.* **2002**, *81*, 1062–1064.
- [33] M. V. R. Murty, S. K. Streiffer, G. B. Stephenson, J. A. Eastman, G. R. Bai, A. Munkholm, O. Auciello, C. Thompson, *Appl. Phys. Lett.* **2002**, *80*, 1809–1811.
- [34] S. K. Streiffer, J. A. Eastman, D. D. Fong, C. Thompson, A. Munkholm, M. V. R. Murty, O. Auciello, G. R. Bai, G. B. Stephenson, *Phys. Rev. Lett.* **2002**, *89*, 067601.
- [35] Y. Masuda, T. Koumura, T. Okawa, K. Koumoto, *J. Colloid Interface Sci.* **2003**, *263*, 190–195.
- [36] A. Nakamura, S. Shigemori, Y. Shimizu, T. Aoki, J. Temmyo, *J. Appl. Phys.* **2004**, *43*, 7672–7676.
- [37] D. M. Hansen, C. E. Albaugh, P. D. Moran, T. F. Kuech, *Appl. Phys. Lett.* **2001**, *79*, 3413–3415.
- [38] R. M. Bozorth, E. F. Tilden, A. J. Williams, *Phys. Rev.* **1955**, *99*, 1788–1798.
- [39] J. Echigoya, S. Hayashi, Y. Obi, *J. Mater. Sci.* **2000**, *35*, 5587–5591.
- [40] G. Srinivasan, E. T. Rasmussen, J. Gallegos, R. Srinivasan, Y. I. Bokhan, V. M. Laletin, *Phys. Rev. B* **2001**, *64*, 214408.
- [41] G. Srinivasan, V. M. Laletin, R. Hayes, N. Puddubnaya, E. T. Rasmussen, D. J. Fekel, *Solid State Commun.* **2002**, *124*, 373–378.
- [42] Y. K. Fetisov, K. E. Kamentsev, A. Y. Ostashchenko, *J. Magn. Mater.* **2004**, *272–276*, 2064.
- [43] H. Zheng, J. Wang, L. Mohaddes-Ardabili, M. Wuttig, L. Salamanca-Riba, D. G. Schlom, R. Ramesh, *Appl. Phys. Lett.* **2004**, *85*, 2035–2037.
- [44] D. Y. Xia, A. Biswas, D. Li, S. R. J. Brueck, *Adv. Mater.* **2004**, *16*, 1427–1432.
- [45] D. Y. Xia, S. R. J. Brueck, *Nano Lett.* **2004**, *4*, 1295–1299.

Received: August 30, 2005
Published online on November 28, 2005